nature water

Article

https://doi.org/10.1038/s44221-025-00542-4

Coupled chemical–microbial deterioration in stagnant fire hydrant branches threatens drinking water quality

Received: 2 August 2025

Accepted: 24 October 2025

Published online: 2 January 2026

Check for updates

Mengqing Fan[1,2,7], Qiang Xu[1,2,7], Xiaoxuan Wang[1,2], Zhiwei Fang[1,2], Mark C. M. van Loosdrecht[3], Martin Pabst[3], Yu Tao[4], Joan B. Rose[5], Walter van der Meer[6] & Gang Liu[1,2]

Fire hydrants are widely installed in drinking water distribution systems, where stagnant water forms multiple 'high-risk zones'. The stagnant water quality at hydrant terminals has been poorly studied. Here we show that stagnant water exhibited an 18-fold increase in manganese, a 40-fold increase in total cell counts, a 13-fold increase in adenosine triphosphate and enrichment of opportunistic pathogens compared with flowing water. Notable changes were also observed in microbial communities and dissolved organic matter composition, including shifts in dominant bacterial taxa, transformation of saturated oxidized compounds and generation of unsaturated reduced compounds. This study also explored the ecological mechanisms underlying the covariation of microorganisms and dissolved organic matter after water stagnation. This finding provides an additional possibility for drinking water quality deterioration in drinking water distribution systems, highlighting the potential threat posed by stagnant water in non-consumer terminals (fire hydrants) to water safety.

In drinking water distribution systems (DWDSs), fire hydrants serve as essential emergency water access points for firefighting and are widely and densely installed throughout urban pipe systems[1,2]. For example, regulations in the USA stipulate a maximum spacing between hydrants of 240 m (ref. 3), with over 9 million hydrants recorded in the database[4]. Canada recommends a maximum spacing of 150 m (ref. 5), while New Zealand requires a maximum spacing of 135 m to ensure adequate fire protection coverage[6]. In China, the maximum spacing is 120 m (ref. 7), with over 2 million hydrants nationwide[8]. Fire hydrants have a critical role in urban safety and are therefore rarely activated during normal operation. As a result, the hydrant body and its connecting branch pipes often remain in a state of low disturbance, low flow or even complete stagnation, thereby forming locations of stagnant water.

Stagnation of drinking water within DWDSs can lead to various water quality problems. Previous studies have shown that stagnation can result in disinfectant decay, microbial regrowth[9], changes in microbial community composition[10–12] and even the presence of opportunistic pathogens[13]. In addition, changes in metal ion concentrations[14,15], increases in disinfection by-products[16,17] and shifts in the composition of dissolved organic matter (DOM) have also been observed[18,19]. However, most existing research on 'stagnant water' has focused on premise plumbing or storage tanks, including stagnation caused by changes in daily water use frequency or temporary absence (such as holiday periods), while non-consumer stagnation zones formed by fire hydrants in DWDSs have received far less attention. The exposure pathway of stagnant water at hydrant and consumer terminals

[1]Key Laboratory of Environmental Aquatic Chemistry, State Key Laboratory of Regional Environment and Sustainability, Research Center for Eco-Environmental Sciences, Chinese Academy of Sciences, Beijing, China. [2]University of Chinese Academy of Sciences, Beijing, China. [3]Department of Biotechnology, Delft University of Technology, Delft, the Netherlands. [4]School of Eco-Environment, Harbin Institute of Technology, Shenzhen, China. [5]Department of Fisheries and Wildlife, Michigan State University, East Lansing, MI, USA. [6]Science and Technology, University of Twente, Enschede, the Netherlands. [7]These authors contributed equally: Mengqing Fan, Qiang Xu. e-mail: gliu@rcees.ac.cn

is fundamentally different. Stagnant water at consumer terminals is regularly consumed, and stagnation periods are relatively short. The associated risk mainly arises through direct water use. By contrast, water in hydrant branches can remain stagnant for much longer periods and may re-enter the main pipelines during sudden pressure changes. In this case, the exposure risk is realized indirectly through its impact on the flowing water in the main pipelines, and the interactions between stagnant and flowing water remain poorly understood. Given the high density and large number of fire hydrants, such areas may form multiple high-risk zones at a spatial scale, posing potential threats to the overall water quality within the DWDSs. Yet, there is still limited understanding of the characteristics of stagnant water in these fire protection terminals, creating a fundamental gap in our comprehension of the associated risks under real-world operating conditions.

The changes occurring in drinking water during stagnation are not limited to microbial growth and DOM consumption but rather reflect a coordinated response of microorganisms and DOM to environmental shifts such as hydraulic conditions and residual chlorine concentrations, governed by complex ecological mechanisms[20–22]. Therefore, beyond quantitatively assessing the variations in microbial and chemical indicators in stagnant water, it is essential to explore the underlying ecological processes driving these changes. The advancement of high-throughput sequencing technologies has greatly facilitated the characterization of microbial community composition and dynamics in DWDSs[23–25], while Fourier transform ion cyclotron resonance mass spectrometry (FT-ICR MS) provides unprecedented resolution for molecular-level analysis of DOM[26–28]. Previous studies have demonstrated that combining these two advanced approaches enables a deeper understanding of the microecological interactions between microorganisms and DOM in aquatic environments[29–31].

To reveal the characteristics of stagnant water in hydrant branches, samples of stagnant and flowing water were collected from 15 fire hydrants in a major city in northern China (Fig. 1a). By integrating high-throughput sequencing and FT-ICR MS analyses, the study addressed three main questions concerning variability after stagnation: (1) Quantitative: how do concentrations of microorganisms (including opportunistic pathogens), DOM and metals vary? (2) Compositional: how do the compositions of microbial communities and DOM vary? (3) Coupling: how do the interactions between microorganisms and DOM vary? This study not only provides a fundamental understanding of the characteristics of stagnant water in hydrant branches but also reveals overlooked yet widespread risk nodes in DWDSs.

Result

Variations in basic parameters

In terms of biomass indicators, the stagnant water exhibited significantly higher microbial biomass than the flowing water ($P < 0.001$; Fig. 1b). Specifically, total cell count (TCC) in stagnant water at each sampling site was consistently on average 40 times higher than in the corresponding flowing water. Similarly, adenosine triphosphate (ATP) levels in stagnant water were, on average, 13 times those in flowing water across all sampling sites. These results indicate that pronounced microbial accumulation occurred in the stagnant water, probably due to the relatively stable hydraulic conditions, which provided a more favourable environment for microbial growth and reproduction, allowing microorganisms to accumulate and proliferate.

Although no significant difference was observed in dissolved organic carbon (DOC) between stagnant and flowing water, the ultraviolet (UV) absorbance at 254 nm (UV_{254}) in stagnant water was significantly higher ($P < 0.001$; Fig. 1c), averaging 1.4 times that of flowing water. This suggests that differences may exist in the properties or composition of DOM between the two water types.

Among the 16 metal elements analysed (Fig. 1d and Supplementary Fig. 1), four metal ions—aluminium (Al), arsenic (As), chromium (Cr) and manganese (Mn)—showed significant differences between stagnant and flowing water ($P < 0.05$). Specifically, the concentrations of Al, As and Cr were lower in stagnant water compared with flowing water, whereas the concentration of Mn was markedly elevated, with an 18-fold increase. This phenomenon suggests that certain metal present in stagnant water also underwent transformation processes, potentially driven by changes in physicochemical conditions, or microbial activity after water stagnation.

Microbial composition analysis

For the bacterial community, alpha diversity in stagnant water was significantly higher than in flowing water ($P < 0.001$; Fig. 2a). Specifically, the average number of observed amplicon sequence variants (ASVs) increased markedly from 719 in flowing water to 4,424 in stagnant water—approximately a sixfold rise. Similarly, the average Shannon diversity index doubled, increasing from 3 to 6. Principal coordinates analysis (PCoA) further revealed a significant overall difference in bacterial community composition between flowing and stagnant water ($P < 0.001$, ADONIS; Fig. 2b), indicating that prolonged water stagnation at the hydrant-associated endpoints has profoundly altered microbial community composition. Further analysis revealed marked differences in the dominant bacterial taxa at the order to genus levels between flowing and stagnant water (Supplementary Fig. 2).

At the genus level, the Venn diagram showed 168 and 598 unique genera in flowing and stagnant water, respectively, with 1,184 shared genera (Fig. 2c). The unique genera exhibited low relative abundance—0.2% in flowing water and 2% in stagnant water—indicating that their contribution to the community's ecological functions may be limited. According to the taxonomic cladograms based on the top 200 genera ranked by relative abundance, Proteobacteria, Firmicutes and Actinobacteriota were the dominant phyla (Fig. 2d). These three phyla accounted for 80.5% of the top 200 genera in flowing water and 65.0% in stagnant water. In addition, genera from Bacteroidota and Planctomycetota accounted for 6% and 5.5%, respectively, in flowing water, while in stagnant water, Planctomycetota, Chloroflexi, Verrucomicrobiota and Bacteroidota contributed 8%, 5.5%, 5% and 4.5%, respectively, suggesting a more even community structure in stagnant conditions. The unique genera in flowing and stagnant water accounted for a small fraction of the high-abundance taxa (top 200 genera, first ring) and were not dominant members of the communities. Only five unique genera were identified in flowing water, belonging to Proteobacteria and Verrucomicrobiota. By contrast, six unique genera were identified in stagnant water, distributed across Proteobacteria, Firmicutes, Chloroflexi, Verrucomicrobiota and other phyla.

Furthermore, we compared the absolute abundances of ten common opportunistic pathogens between the two water types (Supplementary Fig. 3). *Aeromonas hydrophila*, *Acinetobacter johnsonii*, enterotoxigenic *Escherichia coli*, *Klebsiella pneumoniae*, *Mycobacterium avium* and *Pseudomonas aeruginosa* were significantly more abundant in stagnant water than in flowing water ($P < 0.05$). *Legionella pneumophila* showed an increasing trend at approximately half of the sites ($n = 8$), whereas *Acinetobacter baumannii* exhibited no consistent pattern. *Bacteroides fragilis* and enterohaemorrhagic *Escherichia coliO157:H7* were not detected in any of the samples.

Spectroscopic and molecular characterization of DOM

Based on excitation-emission matrix parallel factor (EEM-PARAFAC) analysis, the relative concentrations of four components (C1–C4) were quantified using F_{max} values (Fig. 3a). A comparison of F_{max} values between flowing and stagnant water at each sampling point revealed that the F_{max} values of components C1, C2 and C4 were significantly higher in stagnant water ($P < 0.05$), further confirming the distinct DOM characteristics between the two water types.

To gain deeper insights, molecular-level characterization of DOM was performed for both flowing and stagnant water at each site. The results showed that the number of molecules detected in stagnant water was significantly higher than in flowing water ($P < 0.05$), with

https://doi.org/10.1038/s44221-025-00542-4

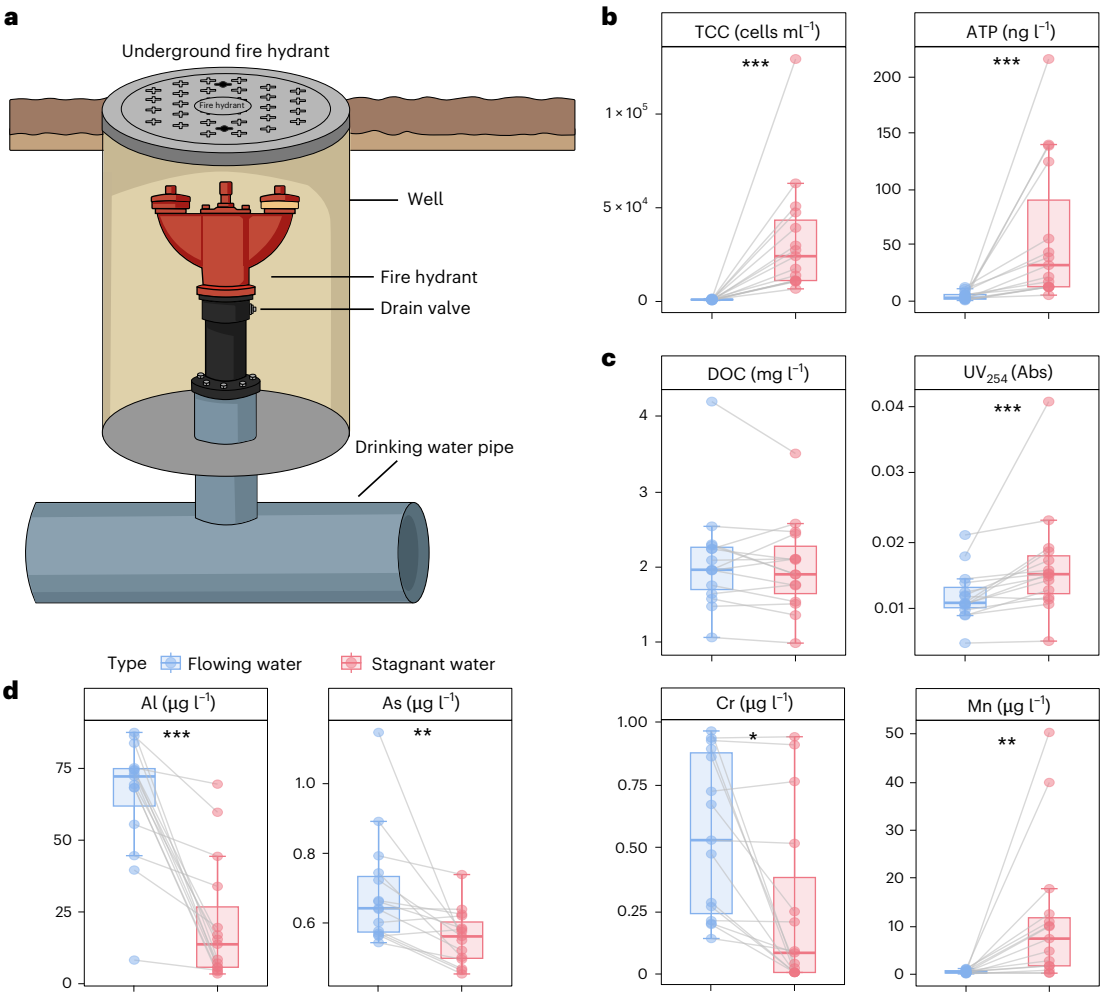

Fig. 1 | Illustration of fire hydrant and chemical-microbial water quality comparison between stagnant and flowing water. a, A schematic diagram of the underground fire hydrant. **b**–**d**, Boxplots showing biomass quantified by TCC and ATP (**b**), DOM characterized by DOC concentrations and UV_{254} (**c**), and metal ions with significant differences between stagnant and flowing water (**d**). The boxes represent the interquartile range (25th–75th percentiles), the horizontal lines inside the boxes indicate the median (50th percentile) and the whiskers extend to the minimum and maximum values within 1.5 times the interquartile range. In **b**–**d**, statistical significance between water types for each index was assessed using two-sided paired Wilcoxon tests, with *P* values adjusted using the Holm method ($n = 15$ per type). Exact *P* values are 0.0002 (TCC), 0.0002 (ATP), 0.27 (DOC), 0.0004 (UV_{254}), 0.0009 (Al), 0.008 (As), 0.015 (Cr) and 0.003 (Mn). $^{*}P < 0.05$, $^{**}P < 0.01$, $^{***}P < 0.001$.

mean values of 2,990 and 3,333, respectively (Fig. 3b). However, no significant difference was observed in the Shannon diversity. PCoA further revealed a significant difference in DOM molecular composition between flowing and stagnant water ($P < 0.001$, ADONIS; Fig. 3c), indicating that long-term stagnation at the distribution system extremities has altered the composition of DOM.

In terms of elemental composition, the number of molecules of CHO, CHON and CHOS was significantly higher in stagnant water, whereas those of CHOCl and CHONP were significantly lower compared with flowing water (Fig. 3d). No significant differences were found in other elemental groups. Regarding relative intensity, molecules of CHOCl, CHONP and CHOP exhibited significantly lower intensities in stagnant water, while the rest showed no significant differences. As for compound category, stagnant water contained significantly more molecules classified as lignin, N-containing saturated compounds (N-ConSatCom) and N-free saturated compounds (N-FreeSatCom). No significant differences were observed for other categories in terms of molecular counts. From the perspective of relative intensity, carbohydrates and tannins were significantly less relative abundant in stagnant water, while no notable differences were detected for the remaining compound categories.

The molecular properties of DOM between the two water types at each sampling point were compared (Supplementary Fig. 4). H/C and O/C ratios provide a direct indication of the hydrogen and oxygen content in molecules. Further, double bond equivalent minus oxygen per carbon ((DBE-O)/C), nominal oxidation state of carbon (NOSC) and modified aromaticity index (AI_{mod}) were used to characterize the degree of unsaturation, redox state and aromaticity, respectively. For a given compound, higher (DBE-O)/C values indicate a greater degree of unsaturation, higher NOSC values reflect a more oxidized state and higher AI_{mod} values correspond to stronger aromaticity. At most sites, the H/C and (DBE-O)/C values in flowing water were generally lower than those in stagnant water, whereas the O/C and NOSC values were generally higher. Paired Wilcoxon signed-rank test results indicated that the differences in these indices between the two water types were statistically significant ($P < 0.05$). By contrast, the AI_{mod} index showed no significant difference or consistent trend between the two water types.

Analysis of unique molecules in the two water types

In-depth analysis of unique molecules helps to reveal the transformation characteristics of DOM after water stagnation. This study integrated molecules of the same water type from different sampling sites, dividing the

https://doi.org/10.1038/s44221-025-00542-4

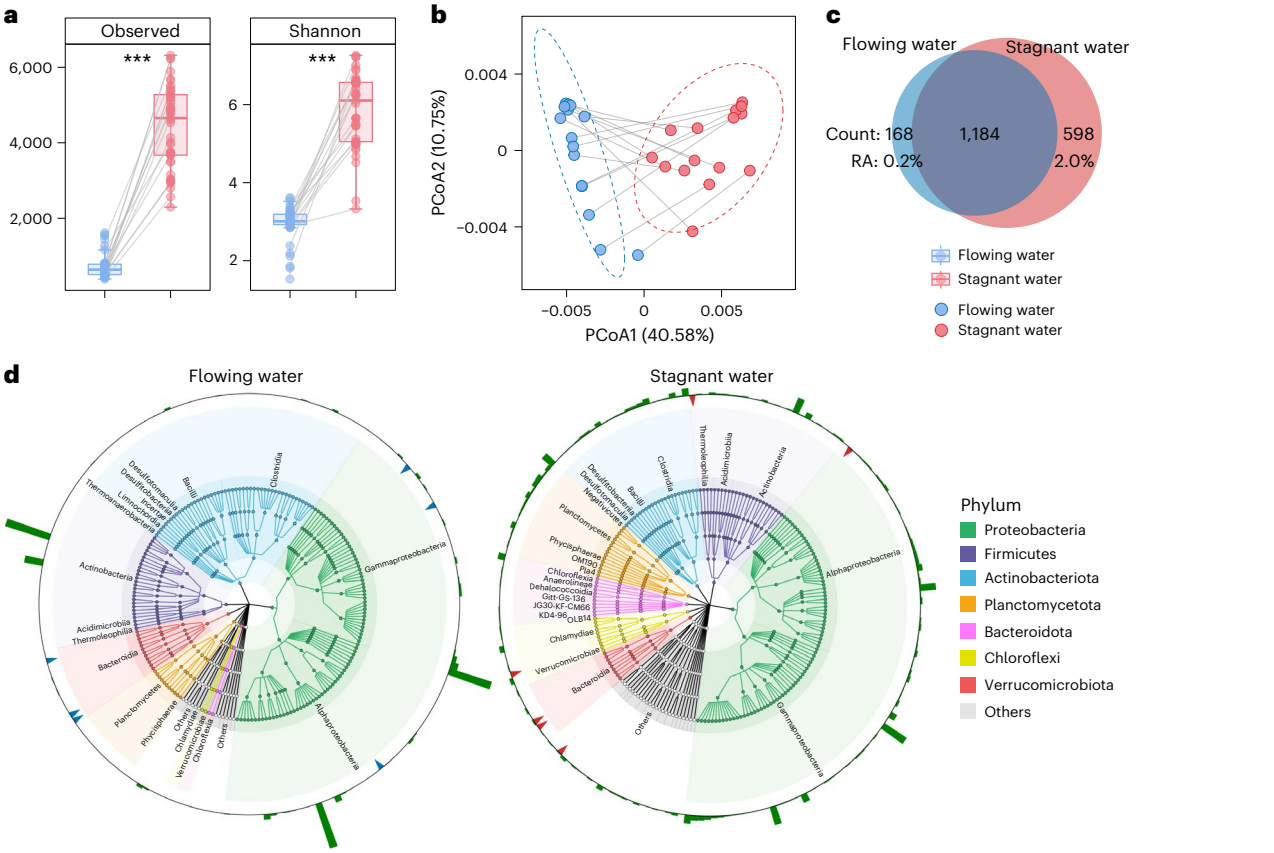

Fig. 2 | Microbial community analysis. a, Boxplots showing microbial community diversity in the two water types. The boxes represent the interquartile range (25th–75th percentiles), the horizontal lines inside the boxes indicate the median (50th percentile) and the whiskers extend to the minimum and maximum values within 1.5 times the interquartile range. Statistical significance between water types for each index was assessed using two-sided paired Wilcoxon tests, with *P* values adjusted using the Holm method ($n = 15$ per type). Exact *P* values are 0.0000 (observed) and 0.0000 (Shannon). **b**, PCoA plot based on Weighted-UniFrac dissimilarity of bacterial community. **c**, Venn diagram of the number of shared and unique genera between flowing water and stagnant water. RA, relative abundance. **d**, Taxonomic cladograms show the top 200 genera based on relative abundance. Class-level names are annotated on the cladograms. The first outer ring uses consistent colours (blue and red) to indicate unique genera to flowing water and stagnant water, respectively. The second outer ring displays the relative abundance of each genus. Note that the taxonomic uniqueness of genera does not necessarily imply high functional importance within the community.

overall molecular pool into three categories: unique molecules in flowing water, unique molecules in stagnant water and shared molecules between the two (Fig. 4a). A total of 4,886 molecules were shared between the two water types, with 723 and 2,105 unique molecules found exclusively in flowing and stagnant water, respectively, and their distribution characteristics differed significantly. In Van Krevelen plots constructed using H/C and O/C, unique molecules in flowing water were primarily located in the right-hand region, while unique molecules in stagnant water were concentrated in the upper-left region. Further analysis using (DBE-O)/C and NOSC as axes, representing the degree of unsaturation and redox state of the molecules, respectively, showed that unique molecules in flowing water were concentrated in the lower-right region, with 38% being saturated oxidized compounds, followed by saturated reduced (28%), unsaturated oxidized (20%) and unsaturated reduced (14%) compounds. By contrast, unique molecules in stagnant water were concentrated in the upper-left region, with 42% being unsaturated reduced molecules, followed by saturated reduced (32%), unsaturated oxidized (15%) and saturated oxidized (11%) molecules.

Regarding elemental composition, unique molecules in flowing and stagnant water showed distinct patterns (Fig. 4b). In flowing water, unique molecules were more diverse, with CHONP (28%), CHON (15%), CHO (12%), CHOS (12%) and CHOP (11%) dominating by count and CHONP (21%), CHOCl (21%), CHON (12%), and CHOP (10%) dominating by abundance. Notably, CHOCl molecules, although fewer in number, contributed significantly to abundance. By contrast, stagnant water showed a more concentrated composition, dominated by CHO (39%), CHOS (33%) and CHON (11%) in count and by CHO (33%), CHOS (31%), and CHONS (11%) in abundance, indicating enhanced formation of sulfur-containing molecules.

The two water types also differed distinctly in compound category, with consistent results in both molecular count and relative abundance. In flowing water, unique molecules were mainly lignin (45% in count, 47% in abundance) and tannins (35% in count, 32% in abundance), while in stagnant water, they were primarily lignin (65% in count, 66% in abundance) and N-FreeSatCom (22% in count, 22% in abundance). By mapping the elemental composition and compound categories onto the NOSC and (DBE-O)/C plots (Supplementary Fig. 5), we found that saturated oxidized compounds (mainly CHONP and CHOCl, tannins) and saturated reduced compounds (mainly CHOP, lignin) in flowing water were transformed during stagnation into unsaturated reduced compounds (mainly CHO, lignin) and saturated reduced compounds (mainly CHOS, N-FreeSatCom).

The study also compared the properties of three types of DOM molecules at each sampling sites (Fig. 4c). For H/C and (DBE-O)/C, the mean values of unique molecules in flowing water were significantly lower than those of shared molecules, with the mean values of shared molecules also significantly lower than those of unique molecules in stagnant water. For O/C and NOSC, the trend was reversed, with the

https://doi.org/10.1038/s44221-025-00542-4

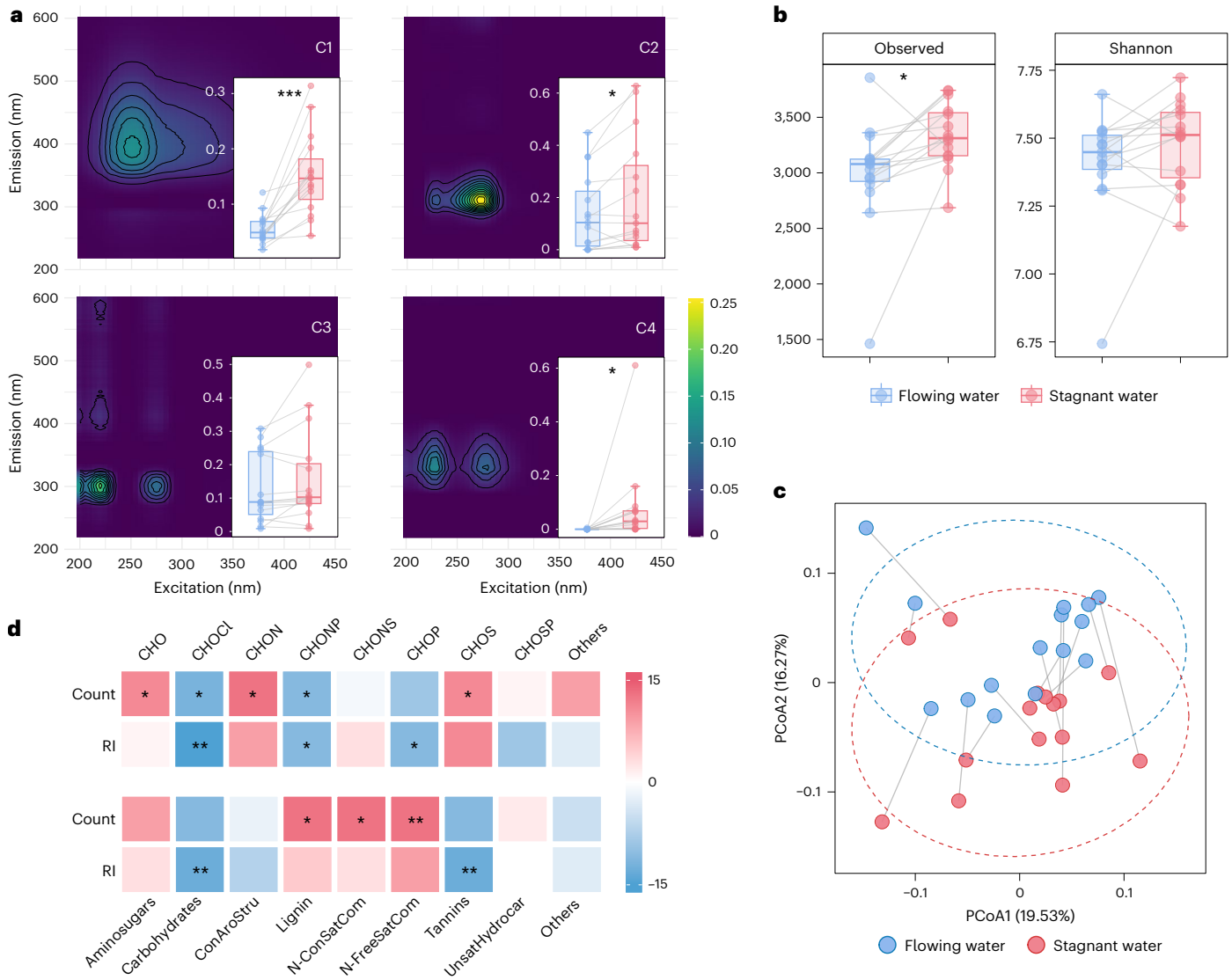

Fig. 3 | Spectroscopic and molecular characterization of DOM. a, Illustration of four fluorescent components (C1, C2, C3 and C4). C1 as a humic-like component[100,101], C2 as a tyrosine-like component[102,103], C3 as a protein-like component[104,105] and C4 as tryptophan-like compounds that have been commonly associated with wastewater and recycled water sources[106–108]. The inset boxplots display the F_{max} values of each component in the two water types ($n = 15$). **b**, Boxplots showing the diversity of DOM molecular composition ($n = 15$). **c**, PCoA plot based on Bray–Curtis dissimilarity of DOM molecular composition. **d**, Deeper red indicates that more samples showed higher values of the given category in stagnant water, while deeper blue indicates more samples with higher values in flowing water. RI, relative intensity. Asterisks indicate significant differences. The boxes represent the interquartile range (25th–75th percentiles), the horizontal lines inside the boxes indicate the median (50th percentile) and the whiskers extend to the minimum and maximum values within 1.5 times the interquartile range. In **a**, **b** and **d**, statistical significance between water types for each index was assessed using two-sided paired Wilcoxon tests, with *P* values adjusted using the Holm method ($n = 15$ per type). Exact *P* values are 0.0002 (C1), 0.011 (C2), 0.11 (C3), 0.01 (C4), 0.02 (observed) and 0.27 (Shannon). $^{*}P < 0.05$, $^{**}P < 0.01$, $^{***}P < 0.001$.

mean values of unique molecules in flowing water being significantly higher than those of shared molecules, and the mean values of shared molecules higher than those of unique molecules in stagnant water. The AI_{mod} index showed no significant differences among the three types of molecules. This result is consistent with the earlier analysis based on the mean differences in molecular properties between the two water types (Supplementary Fig. 4), further supporting the important role of unique molecules in distinguishing the characteristics of the two water types.

Combined analysis of microbial and DOM composition

To explore the relationship between microorganisms and DOM, we first analysed the correlation of their diversity indices for the two water types (Fig. 5a). In flowing water, a significant positive correlation was observed between the observed number of DOM molecules and microbial ASVs ($R = 0.62$, $P < 0.05$), whereas their Shannon diversity showed no significant correlation ($R = -0.10$, $P > 0.05$). By contrast, in stagnant water, not only was the ASV/molecule richness significantly correlated ($R = 0.56$, $P < 0.05$), but a significant positive correlation was also observed between their Shannon diversity indices ($R = 0.53$, $P < 0.05$), which suggests that microbial and DOM compositions are more tightly linked in stagnant water.

After knowing the diversity-based coupling, we further investigated their ecological assembly processes using the beta nearest taxon index (βNTI) to assess microbial and metabolite (DOM) community assembly patterns (Fig. 5b,c). In flowing water, most microbial βNTI values were less than 2, indicating that community assembly was primarily governed by stochastic process and homogeneous selection. By contrast, metabolites exhibited almost exclusively βNTI values

https://doi.org/10.1038/s44221-025-00542-4

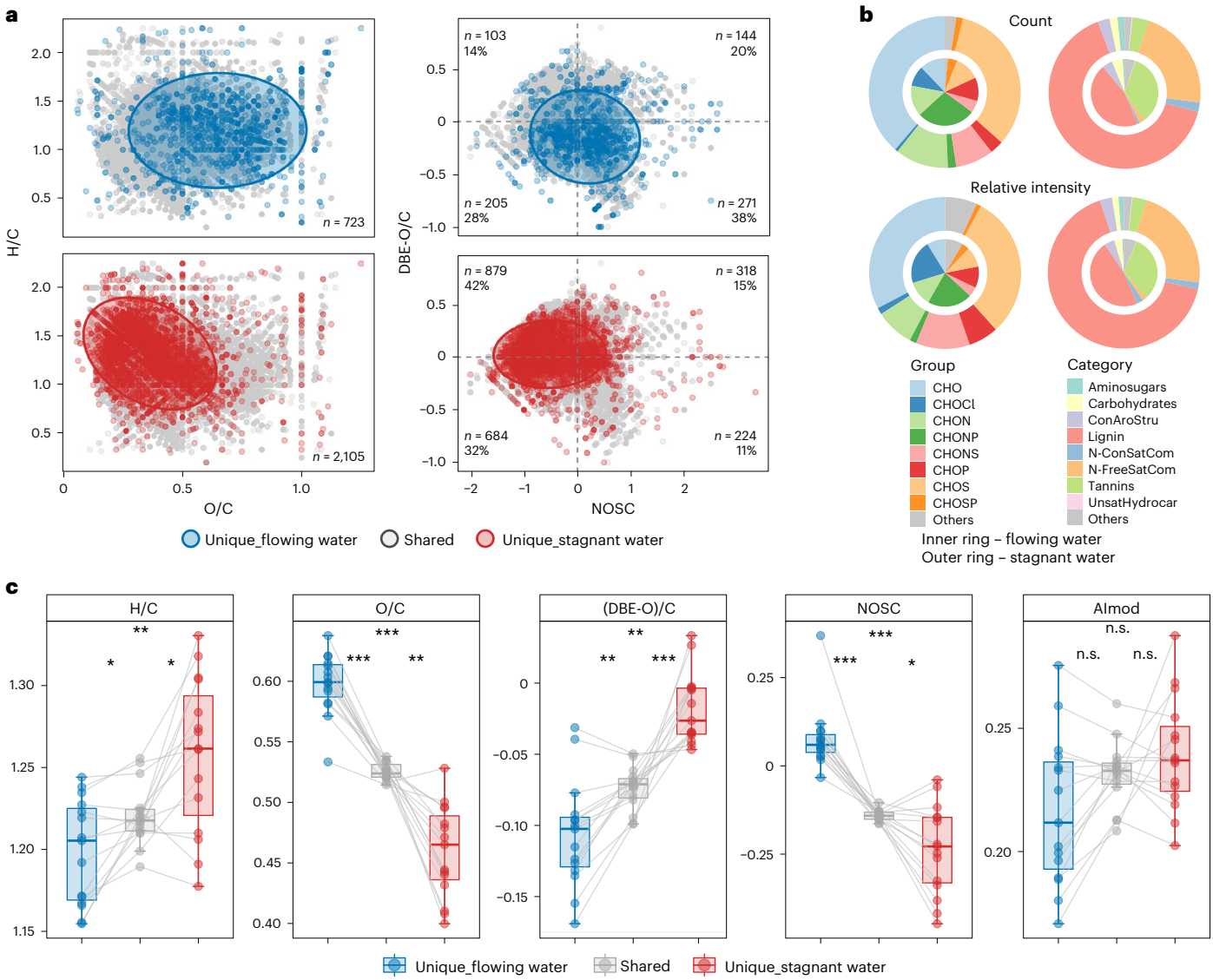

Fig. 4 | Analysis of unique molecules in two water types. a, Overall distribution of unique and shared molecules across all samples, shown with O/C versus H/C and NOSC versus (DBE-O)/C plots. **b**, Elemental composition and compound category distribution of unique molecules in the two water types, shown by both molecular counts and relative intensity. **c**, Comparison of the mean values of key molecular properties for three types of molecular groups across samples ($n = 15$). The boxes represent the interquartile range (25th–75th percentiles), the horizontal lines inside the boxes indicate the median (50th percentile) and the whiskers extend to the minimum and maximum values within 1.5 times the interquartile range. Statistical significance between water types for each index was assessed using two-sided paired Wilcoxon tests, with P values adjusted using the Holm method ($n = 15$ per type). The first layer of significance markers indicates differences in the properties of unique molecules between the two water types, while the second layer indicates differences between unique and shared molecules within flowing or stagnant water. Exact adjusted P values are shown from left to right for each comparison: H/C (0.012, 0.007, 0.035), O/C (0.0009, 0.0009, 0.0012), DBE-O/C (0.0049, 0.0027, 0.0009), NOSC (0.0009, 0.0009, 0.035) and AI_{mod} (0.128, 0.09, 0.72). n.s., not significant. $^{*}P < 0.05$, $^{**}P < 0.01$, $^{***}P < 0.001$.

greater than 2, reflecting strong heterogeneous selection. However, in stagnant water, microbial βNTI values increased markedly, with the majority greater than −2 and 52% exceeding 2, indicating an increasing influence of heterogeneous selection. Similarly, the proportion of DOM governed by heterogeneous selection rose from 95% to 100%. This convergence in assembly mechanisms further supports that prolonged water stagnation at pipe ends promotes stronger coupling between microbial and chemical communities.

Based on the above analysis, we found that microorganisms and DOM underwent notable interactions during the transition from flowing to stagnant water. Therefore, we further performed correlation analysis using the abundance differences of each microbial ASV and DOM molecule between stagnant and flowing water at each sampling site and constructed a bipartite co-occurrence network (Fig. 5d). This network included 1,519 nodes and 1,387 edges, comprising 1,117 ASVs and 402 DOM molecules. Notably, the network exhibited a high degree of modularity (modularity well above 0.4), with six major modules identified, while the remaining modules were relatively small. These six major modules may represent dominant metabolic or resource utilization pathways during the stagnation period. Based on within- and among-module connectivity, the network comprised 0 network hubs, 21 module hubs and 207 connectors, and the remainder were classified as peripheral nodes. Notably, all module hubs in the bipartite network were DOM molecules (Fig. 5e), indicating that, after drinking water stagnation, DOM had a central role in organizing microbial–DOM interactions and shaped a resource-centric network structure.

https://doi.org/10.1038/s44221-025-00542-4

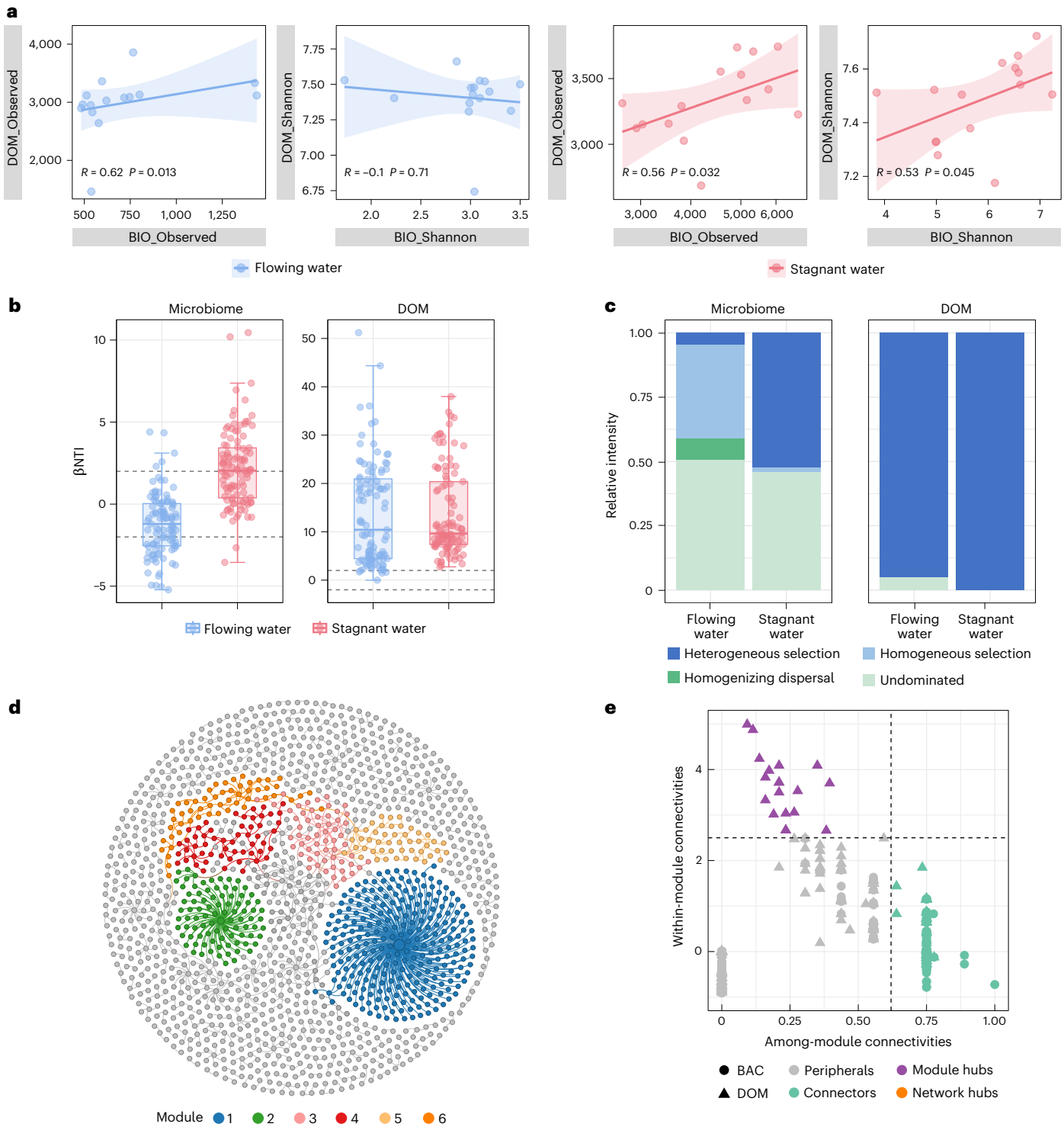

Fig. 5 | Analysis of microbial and DOM diversity, community assembly and co-occurrence network. a, Spearman's correlation analysis of microbial (BIO) and DOM diversity in flowing and stagnant water. The Spearman correlation coefficient (*R*) and associated *P* values are shown for each panel. Points represent individual samples. Solid lines indicate linear regression fits for visualization of the trends, and shaded areas denote the 95% confidence intervals of the fitted lines. **b**, Boxplots showing the within-habitat βNTI results for microbial communities and DOM metabolites (for example, only flowing water-to-flowing water comparisons, $n = 15$). The boxes represent the interquartile range (25th–75th percentiles), the horizontal lines inside the boxes indicate the median (50th percentile) and the whiskers extend to the minimum and maximum values within 1.5 times the interquartile range. **c**, Bar plots showing the putative influence of different ecological processes to the assembly of microbial communities and DOM metabolites in each water type. **d**, Co-occurrence network between bacterial ASVs and DOM molecules. The network topology highlights the top six modules, each shown in a different colour. **e**, Node importance identified by within-module and among-module connectivity. BAC, bacteria.

Discussion

By integrating advancements in analytical chemistry and molecular microbiology, this study focuses on the densely distributed hydrant endpoints within DWDSs, investigating the biological and chemical characteristics of their associated flowing and stagnant water. The findings reveal that water stagnation induces notable changes in microbial community, DOM composition and the covariant succession between microorganisms and metabolites. These results highlight that hydrants as non-consumer terminals may represent overlooked yet widespread risk nodes in DWDSs. This study provides an additional perspective on the potential compound risks in the drinking water distribution process.

Chemical and microbial responses to hydrant stagnation in DWDSs

During stagnation in the DWDSs, drinking water can lose free chlorine within a short time (typically at various times during the day[32]), creating favourable conditions for microbial growth. In this study, all stagnant water samples showed significantly higher microbial biomass than their flowing water samples, with TCC and ATP levels increasing by approximately 40-fold and 13-fold, respectively. These results highlight that stagnant water serves as a hotspot of microbial activity[9,10,12]. Moreover, the discrepancy between TCC and ATP indicates that a considerable fraction of the microbial community in stagnant water may be metabolically inactive, including dormant states[33,34]. Given the mandated density of terminal points such as fire hydrants (with maximum spacing typically limited to a few hundred metres[3,5,6]), this finding provides an additional possibility beyond the conventional view that biomass accumulation in DWDSs is primarily governed by regrowth, biofilms or particles[35–37]. More concerning is the increased abundance of several opportunistic pathogens in stagnant water, including *Aeromonas hydrophila*, *Acinetobacter johnsonii*, enterotoxigenic *Escherichia coli*, *Klebsiella pneumoniae*, *Mycobacterium avium*, *Pseudomonas aeruginosa* and *Legionella pneumophila*. Although the extent of increase varied across sites, this finding suggests that hydrant branches constitute densely distributed hotspots of biological risk within DWDSs, underscoring the need for further investigations into the interactions between stagnant and flowing water, as well as the persistence, viability and potential for regrowth of opportunistic pathogens once introduced into the main pipelines. Consistent with previous studies, community succession also occurred in the stagnant water at the terminals[11,38]. These changes may be driven by chlorine decay that favours chlorine-sensitive taxa[39,40], alterations in dissolved oxygen levels[41] and shifts in DOM composition[42,43]. In addition, the substantial increase in microbial diversity may reflect the introduction of new microbial sources into drinking water, such as the release of biofilm and sediments or microbial contamination during hydrant installation[38,44]. However, these unique genera were of low abundance, indicating that their contribution to the community's ecological functions may be limited. This suggests that the dominant taxa in stagnant water may primarily arise from the succession of pre-existing communities in the drinking water.

Owing to the stagnant water being a long-standing, closed environment, the consumption of dissolved oxygen promotes the formation of local reducing conditions. Our study confirms this hypothesis. Under anoxic conditions, Mn^{2+} is thermodynamically stable and highly soluble in water[45]. Under reducing conditions in stagnant water, Mn oxides—derived from either Mn deposition[46] or corrosion products of ductile cast iron[47]—are chemically and biologically reduced to dissolved Mn^{2+} (refs. 48,49). By contrast, under similar reducing conditions, As(V) is reduced to As(III), with the change in solubility possibly attributed to the accompanying pH variation[50,51]. Meanwhile, the decreases in Al and Cr concentrations in stagnant water may primarily be due to adsorption[14].

Both spectroscopic and molecular perspectives revealed significant differences in DOM between stagnant and flowing water. The stagnation process not only led to a marked increase in DOM diversity but also drove its transformation towards more unsaturated and more reduced molecular compositions. A previous study has shown that reduced, unsaturated, aromatic moieties lead to high-toxicity disinfection by-products (DBPs) formation[52], highlighting the potential risk if such stagnant water enters the main pipelines and reacts with disinfectant. The decrease in the NOSC indicates that the removal of electrons from DOM becomes thermodynamically less favourable, suggesting lower biodegradability[53]. These findings are highly consistent with observations from hypoxic fjord seawater[54], where declining oxygen concentrations corresponded to increased DOM diversity, accumulation of unsaturated and reduced molecules, and diminished thermodynamic degradability. This suggests that oxygen depletion is also a key driver of DOM changes following water stagnation in DWDSs. In addition, the study revealed that saturated oxidized compounds (mainly CHONP and CHOCl, tannins) and saturated reduced compounds (mainly CHOP, lignin) in flowing water were transformed during stagnation into unsaturated reduced compounds (mainly CHO, lignin) and saturated reduced compounds (mainly CHOS, N-FreeSatCom). This indicates that DOM changes in stagnant water involve not only functional group modifications but also substantial molecular reassembly. These unique DOM molecules increase the complexity of disinfection by-product formation in the drinking water of main pipelines, and their post-chlorination toxicity warrants further investigation. In addition, we observed a decrease in phosphorus-containing DOM in stagnant water, which may be attributed to microbial degradation, as microorganisms can convert organic phosphorus into inorganic phosphorus for their own use, representing a major source of inorganic phosphorus in groundwater[55]. Meanwhile, an enrichment of sulfur-containing DOM was also detected in stagnant water. According to previous studies[56], this may be attributed to sulfurization reactions of DOM following oxygen depletion, during which sulfate becomes the primary electron acceptor and inorganic sulfur is incorporated into DOM.

Coupled microbial–chemical evolution after drinking water stagnation

The chemical and microbial properties of stagnant water changed substaintially. According to previous studies, these microbial and chemical changes are not independent but covary[57,58]. In flowing water, owing to the shared source of microorganisms and DOM (for example, the same water treatment processes and distribution system pathways), a certain level of consistency is observed at richness. However, owing to the short hydraulic retention time and the continuous inhibitory effects of residual chlorine on microorganisms, an effective ecological coupling in terms of community composition has not been established. Previous studies have also indicated that residual chlorine is a key factor influencing chemical–biological processes in water[59,60]. During stagnation, more intensive interactions between microorganisms and DOM occur, leading to significant correlations in both microbial richness and community composition (including abundance), which is consistent with previous findings in fresh water[61].

The ecological assembly results further revealed changes in microbial and metabolite communities after water stagnation[62,63]. In flowing water, microbial communities were shaped by both homogeneous selection and stochastic processes, while DOM was mainly influenced by heterogeneous selection, indicating a decoupling between their assembly drivers[64]. At the treatment plant outlet, similar processes led to convergence of microbial communities at some sites. Along the distribution system, differences in pipe material and hydraulics increased stochasticity and community divergence. By contrast, DOM was more sensitive to environmental factors such as pipe material, and residence time, leading to environment-driven differentiation—consistent with patterns observed in permafrost thaw and mudflat intertidal study[64,65]. In stagnant water, both microbial and DOM βNTI values increased, showing more similar assembly responses, supporting their coupled shifts under prolonged stagnation. Heterogeneous

selection dominated in stagnant zones, reflecting internal heterogeneity driven by differences in stagnation time, hydraulic conditions and environmental factors (pH, microelements or toxic metals)[66].

The bipartite co-occurrence network based on abundance differences between microorganisms and DOM provided more intuitive evidence of their coupling. The network exhibited a high degree of modularity. Previous studies have indicated that a module within one network can be regarded as a functional unit that may perform similar ecological tasks[67,68]. For example, microbial taxa within a given module may cooperate in the degradation of specific types of DOM[69]. Note that significant correlations do not necessarily imply actual metabolic relationships, but they can provide useful directions for future experimental studies. However, unlike previous studies[69,70], all module hubs in our network were DOM molecules, suggesting that a few DOM compounds may act as key metabolic or multifunctional substrates, thereby occupying central positions in biochemical transformations and forming a resource-dominant network. This pattern may be attributed to the continuous depletion of DOM and the lack of external inputs under water stagnation, leading to nutrient limitation[71,72]. Moreover, as indicated by our previous analysis, hypoxic conditions reduced the thermodynamic degradability of DOM. The composition of DOM not only profoundly influenced microbial community structure, but also probably drove microbial niche differentiation by shaping resource utilization preferences[73–75]. Together, DOM is probably the dominant selective pressure in stagnant drinking water, shaping microbial niche occupation and community assembly.

Implications and outlook

This study is an innovative investigation of the densely distributed hydrant endpoints within DWDSs. By integrating microbiome and DOM analysis, we systematically compared the microbial and metabolic compositions of flowing and stagnant water, revealing ecological mechanisms underlying the covariant microbial–metabolite succession following water stagnation. While previous studies have primarily focused on microbial regrowth and biofilm release[76,77], our results demonstrate that hydrant endpoints, owing to prolonged stagnation, exhibit rapid chlorine decay and oxygen depletion, becoming hidden 'hotspots' for microbial enrichment and intensified metabolic activity.

Importantly, the 'stagnation water' in this study does not strictly originate from a single water phase. In areas of long-term stagnation, such as the 'dead zones' in hydrants, the boundaries between phases become blurred owing to continuous diffusion, biological activity and other factors. Some biofilms, sediments and corrosion products are in a loose state, and any changes in flow rate or pressure can lead to the redistribution of these components, which then enter the water. Therefore, the stagnation water collected in this study is not a single water phase, but rather a mixture of various loose components, which more accurately reflects the potential risks associated with dead zones. Under normal flow conditions, contaminant migration is primarily diffusion-limited. However, when hydraulic integrity is compromised (for example, pipe breaks, maintenance activities and intermittent supply) or when transient negative pressures occur (for example, intermittent pump activation, valve slamming or failures), contaminants may be rapidly introduced into the main flow. Importantly, although the contribution from an individual hydrant branch is limited, numerous and dense distribution of hydrants can produce cumulative effects that pose non-negligible risks to overall distribution system water quality. It is worth noting that this study does not quantify the actual impact of these zones on the DWDS. Sampling in this investigation does not capture the stable biofilm communities on the pipe walls, which imposes certain limitations on the discussion of microbial risks and ecological processes in hydrant stagnation zones. A more complete understanding of the ecosystem in hydrant branches therefore requires direct sampling of biofilms in the future, for example, by collecting attached communities after flushing. Water utilities generally lack awareness of interventions for managing these dense stagnation zones in hydrant branches. Based on our findings about water deterioration, we call for further research to help inform the establishment of appropriate flushing frequencies and mandatory management strategies for hydrant terminals. We also recommend that researchers or water utilities incorporate sensitive and rapid indicators, such as TCC, ATP and excitation-emission matrices (EEMs), into future studies or monitoring efforts, for example, to track deterioration in stagnation zones or to assess the impact of pressure fluctuations on water quality in the main pipelines.

Although this study provides field-based comparisons between flowing and stagnant water, the static sampling design does not capture the dynamic interactions between the two, nor does it assess the effects of influencing factors such as flow rate or pipe diameter. Future studies should incorporate controlled simulation experiments, including computational fluid dynamics modelling, to examine the potential impact of stagnant water backflow or mixing on flowing water quality and to elucidate the mechanisms of risk propagation under varying hydraulic conditions. In addition, while our study identified key environmental indicators such as dissolved oxygen and redox potential, further quantitative analysis is needed to clarify their roles. Integrating environmental factors, multi-omics analysis and dynamic simulation will be essential in future research to uncover the functional and expression-level mechanisms governing microbial–chemical cosuccession at non-consumer terminals, as well as their interactions with the main water supply. In addition, health data are also essential, and it is necessary to investigate whether areas with high fire hydrant density have a higher incidence of diseases related to drinking water.

Methods

Site description and sample collection

This study was conducted in a city in northern China, where the municipal drinking water supply is primarily sourced from both surface water and groundwater. The municipal drinking water undergoes a comprehensive treatment process consisting of pre-ozonation, coagulation, sedimentation, sand filtration, activated carbon filtration and chlorine disinfection. The city has approximately 81,000 fire hydrants, from which we selected 15 representative sites covering a broad geographic range—from the city centre to suburban areas and from northern to southern regions. At each site, both stagnant and flowing water samples were collected from fire hydrants. All the fire hydrants in the city are installed underground (Fig. 1a), standardized as model SA100/65-1.6 and made of ductile cast iron. To prevent freezing, the hydrants are equipped with a drain valve, which automatically empties the water in the upper red section after the outlet is closed. Therefore, stagnant water is mainly found in the black section of the hydrant below the drain valve and in the branch pipes connected to the main supply line. During sampling, the fire hydrant was first fully opened to allow high-pressure water to flush out potential contaminants from around and inside the hydrant outlet. After a few seconds, the valve was partially closed to allow stagnant water to flow out steadily. Once the flow stabilized, the stagnant water sample was collected. After sampling, the hydrant was fully reopened to flush out any remaining stagnant water. To eliminate potential interactions, we ensured that, after the stagnant water sample was collected, a large volume of residual stagnant water (exceeding twice the sample volume) could still be flushed out. Otherwise, the sampling site was discarded. When the water ran clear and a chlorine odour was detectable, the hydrant was allowed to flow steadily for an additional 10 min before residual chlorine was measured consecutive times. Once the readings stabilized, the flowing water was collected, and the residual chlorine concentrations for each site were recorded (Supplementary Table 1). At each site, each type of water sample was collected in triplicate (three subsamples, totalling 4.5 litres) using black plastic containers lined with polytetrafluoroethylene[78,79].

Samples were kept in the dark and transported under cooled conditions to the laboratory.

Please note that, for each sampling point and each water type, three biological replicates were collected ($n = 15 \times 2 \times 3 = 90$). All subsequent analyses were based on these three biological replicates ($n = 90$), except for FT-ICR MS, which was performed on three pooled replicates ($n = 30$).

Characterization of metal ions

Metals (Al, Fe, Mn, Cu, Zn, As, Cr, Cd, Hg, Pb, Se, Ni, Co, Sn, Sb and Ba) were analysed using inductively coupled plasma mass spectrometry (Thermo Scientific, iCAP RQ). Before analysis, 10 ml of each water sample was filtered through a 0.45-µm membrane and acidified with 0.1 ml of concentrated nitric acid. The method detection limits are summarized in Supplementary Table 2.

Biomass quantification

TCC. TCC in water samples were quantified using a flow cytometer (Agilent NovoCyte 1040) following established protocols[80–82]. In brief, 1 ml of sample was stained with 10 µl ml^{-1} SYBR Green I (1:100 dilution in dimethyl sulfoxide), incubated in the dark at 35 °C for 10 min and then analysed.

ATP. ATP levels were measured using a GloMax Navigator Microplate Luminometer (Promega) with Water-Glo Detection Reagent as described previously[83]. Each 500-µl water sample was mixed with 500 µl lysis reagent, incubated at room temperature for 2 h, and 125 µl was transferred to a 96-well plate for triplicate measurements. ATP concentrations were calculated using a standard curve ($R^2 > 0.99$).

DNA extraction, quantitative PCR and amplicon sequencing

A total of 1,000 ml water was filtered through a 0.22-µm membrane filter (Whatman), and the filters were stored at −20 °C until DNA extraction. DNA was extracted using the FastDNA SPIN Kit for Soil (MP Biomedicals) following the manufacturer's instructions.

Quantitative PCR assays were conducted on a CFX96 Real-Time PCR System (Bio-Rad) using the TaqMan probe chemistry. Ten opportunistic pathogens commonly associated with drinking water were targeted: *Acinetobacter baumannii*, *Aeromonas hydrophila*, *Acinetobacter johnsonii*, *Bacteroides fragilis*, enterohaemorrhagic *Escherichia coli O157:H7*, enterotoxigenic *E. coli*, *Klebsiella pneumoniae*, *Legionella pneumophila*, *Mycobacterium avium* and *Pseudomonas aeruginosa*. Experimental details, including methods, primers/probes and reaction conditions, are provided in the Supplementary Information (Supplementary Text 1 and Supplementary Tables 3 and 4).

The V3–V4 region of the 16S rRNA gene was amplified using primers 341 F (5′-CCTACGGGNGGCWGCAG-3′) and 785 R (5′-GACTACHVGGGTATCTAATCC-3′)[84]. PCR products were purified and sequenced on the Illumina Nova 6000 platform (Guangdong Magigene Biotechnology) to generate 2 × 250 bp paired-end reads. Raw reads were trimmed to remove primers using Cutadapt v3.1 (ref. 85). Quality control, denoising, read merging, chimera removal and ASV table construction were performed using DADA2 v1.21.0 (ref. 86). Taxonomic assignment and phylogenetic analysis were carried out with QIIME2 v2020.11 (ref. 87).

DOM quantification and fluorescence analysis

Water samples were prefiltered through GF/F filters (nominal pore size 0.7 µm)[28,88]. DOC was measured using a Shimadzu TOC-L analyser (detection limit 0.01 mg l^{-1}, precision ±2%). UV_{254} was determined with a Cary 60 UV–vis spectrophotometer (Agilent) using a 1-cm quartz cuvette. As all absorbance values at 254 nm were below 0.3 (ref. 89), fluorescence EEMs were measured directly using an F-7000 spectrofluorometer (Hitachi). Excitation wavelengths ranged from 200 nm to 450 nm (5-nm steps), and emission wavelengths from 220 nm to 600 nm (2-nm steps). The detector voltage and scan speed were set to 700 V and 12,000 nm min^{-1}, respectively.

EEM data were processed using the StaRDOM package in R (ref. 90), including blank subtraction, Raman normalization and removal of Rayleigh and Raman scatter. Parallel factor analysis (PARAFAC) was used to extract four fluorescent components (C1–C4), which were compared with the OpenFluor database (https://openfluor.lablicate.com). All matched components had excitation and emission similarity scores above 0.95.

FT-ICR MS analysis

Collected 300-ml water samples were acidified to pH 2.0 using formic acid (HCOOH) and subjected to solid-phase extraction. Agilent Bond Elut-PPL cartridges (500 mg, 6 ml) were preconditioned with 12 ml methanol, followed by 12 ml of acidified ultrapure water (pH 2, HCOOH). Samples were loaded onto the cartridges at a flow rate of 5 ml min^{-1}. After loading, cartridges were rinsed with 12 ml of acidified ultrapure water to remove salts and dried under a nitrogen stream. The retained compounds were eluted with 12 ml of methanol, and the eluates were blow-dried with nitrogen, redissolved in 1 ml of methanol and stored in the dark at −20 °C. Notably, formic acid was used instead of hydrochloric acid to avoid chloride adduct formation between chloride ions and DOM[91,92].

The molecular composition of DOM was analysed using a 15.0 Tesla Bruker Solarix FT-ICR MS (Bruker Daltonics) equipped with a negative electrospray ionization source. Detailed analytical conditions and data analysis procedures are provided in Supplementary Texts 2 and 3, respectively. The criteria for DOM molecule categorization are presented in Supplementary Table 5.

Statistical analysis

Alpha and beta diversity. The alpha diversity of bacteria was calculated using observed ASV number (Observed), and Shannon–Wiener (Shannon) indices. For DOM, relative peak intensities were calculated by normalizing each peak to the total intensity per sample, and the alpha diversity of DOM was calculated using observed molecule number (observed), and Shannon–Wiener (Shannon) indices. In the bar plots of microbial biomass, DOC, opportunistic pathogens, alpha diversity and fluorescent components for the two water types, connecting lines indicate samples from the same site, and statistical significance was assessed using paired Wilcoxon tests. Beta diversity was analysed using Weighted-Unifrac (bacteria) and Bray–Curtis (DOM) dissimilarity and visualized with PCoA. Differences in bacterial and DOM composition between flowing and stagnant water were tested using ADONIS (permutational multivariate analysis of variance, PERMANOVA). All analyses were performed with the vegan package[93].

Ecological assembly process. Ecological assembly processes of microbial and metabolite communities were assessed using βNTI and Raup–Crick Bray–Curtis index (RCbray), calculated with the NST package[94]. According to previous studies[62,64,95,96], when $|\beta NTI| > 2$, deterministic processes dominate community assembly: $\beta NTI > 2$ indicates heterogeneous selection, where divergent environmental conditions drive high community turnover; $\beta NTI < -2$ indicates homogeneous selection, where stable environmental pressures lead to low turnover. When $|\beta NTI| < 2$, stochastic processes are considered predominant. In these cases, RCbray was used to further distinguish the underlying mechanisms: $|RCbray| < 0.95$ indicates undominated assembly; $RCbray > 0.95$ reflects dispersal limitation; $RCbray < -0.95$ represents homogenizing dispersal.

Co-occurrence network. Co-occurrence networks were built using the differences in relative abundance of microbial ASVs and DOM molecules between stagnant and flowing water. ASVs and molecules in fewer than half of the samples were excluded. *P* values were adjusted with the Benjamini–Hochberg method[97]. Strong correlations ($|\rho| \geq 0.8$, $P < 0.05$) were used to construct bipartite networks, visualized and

clustered in Gephi (https://gephi.org). Nodes have been divided into four categories[98]: (1) peripheral nodes (Zi ≤2.5, Pi ≤0.62), (2) connectors (Zi ≤2.5, Pi >0.62), (3) module hubs (Zi >2.5, Pi ≤0.62) and (4) network hubs (Zi >2.5, Pi >0.62). All the statistical analyses were performed in R (version 4.3.1, R Core Team, 2023).

Reporting summary

Further information on research design is available in the Nature Portfolio Reporting Summary linked to this article.

Data availability

Sequence data associated with this project have been deposited in the National Center for Biotechnology Information (NCBI) Short Read Archive database (accession number PRJNA1267700). FT-ICR MS raw data are available via Zenodo at https://doi.org/10.5281/zenodo.17422657 (ref. 99). Source data are provided with this paper.

Code availability

All codes used in this study are available in the Article or its Supplementary Information.

References

1. Raškauskaitė, R. & Grigonis, V. An approach for the analysis of the accessibility of fire hydrants in urban territories. *ISPRS Int. J. Geo-Inf.* **8**, 587 (2019).
2. Abrar, A., Kamal, A. S. M. M. & Fahim, A. K. F. Fire risk vulnerability and safety assessment of Farmgate area using fire risk index, Dhaka City and optimization of fire hydrant placement. *Progress Disast. Sci.* **24**, 100384 (2024).
3. *NFPA 1: Fire Code. Section 18.5* (National Fire Protection Association, 2024).
4. *ISO's PPC Database Reaches 9 Million Hydrants* (Verisk, 2018).
5. *Water Supply for Public Fire Protection: A Guide to Recommended Practice in Canada* (Fire Underwriters Survey, 2020).
6. *New Zealand Fire Service Firefighting Water Supplies Code of Practice* (National Commander New Zealand Fire Service, 2008).
7. *Technical Code for Fire Protection Water Supply and Hydrant Systems* (Ministry of Housing and Urban–Rural Development of the People's Republic of China, 2014).
8. "14th Five-Year" National Fire Protection Work Plan. *Ministry of Emergency Management of the People's Republic of China* https://www.mem.gov.cn/gk/zfxxgkpt/fdzdgknr/202204/P020220414388243662697.pdf (2022).
9. Prest, E. I., Hammes, F., Kotzsch, S., van Loosdrecht, M. C. & Vrouwenvelder, J. S. Monitoring microbiological changes in drinking water systems using a fast and reproducible flow cytometric method. *Water Res.* **47**, 7131–7142 (2013).
10. Zlatanovic, L., van der Hoek, J. P. & Vreeburg, J. H. G. An experimental study on the influence of water stagnation and temperature change on water quality in a full-scale domestic drinking water system. *Water Res.* **123**, 761–772 (2017).
11. Ling, F., Whitaker, R., LeChevallier, M. W. & Liu, W. T. Drinking water microbiome assembly induced by water stagnation. *ISME J* **12**, 1520–1531 (2018).
12. Lautenschlager, K., Boon, N., Wang, Y., Egli, T. & Hammes, F. Overnight stagnation of drinking water in household taps induces microbial growth and changes in community composition. *Water Res.* **44**, 4868–4877 (2010).
13. Huang, C. K. et al. Extended water stagnation in buildings during the COVID-19 pandemic increases the risks posed by opportunistic pathogens. *Water Res X* **21**, 100201 (2023).
14. Zhang, S. et al. Study on release and occurrence of typical metals in corrosion products of drinking water distribution systems under stagnation conditions. *Environ. Sci. Pollut. Res. Int.* **30**, 15217–15229 (2023).
15. Ghoochani, S., Salehi, M., DeSimone, D., Salehi Esfandarani, M. & Bhattacharjee, L. Studying the impacts of non-routine extended schools' closure on heavy metal release into tap water. *Environ. Sci. Water Res. Technol.* **8**, 1223–1235 (2022).
16. Dion-Fortier, A., Rodriguez, M. J., Serodes, J. & Proulx, F. Impact of water stagnation in residential cold and hot water plumbing on concentrations of trihalomethanes and haloacetic acids. *Water Res.* **43**, 3057–3066 (2009).
17. Kurajica, L., Ujević Bošnjak, M., Kinsela, A. S., Štiglić, J. & Waite, T. D. Heavy metal, organic matter, and disinfection byproduct release from drinking water pipe scales under stagnant conditions. *Environ. Sci. Water Res. Technol.* **9**, 235–248 (2023).
18. Maqbool, T. et al. Fluorescence moieties as a surrogate for residual chlorine in three drinking water networks. *Chem. Eng. J.* **411**, 128519 (2021).
19. Zhang, H. H. et al. Indoor heating drives water bacterial growth and community metabolic profile changes in building tap pipes during the winter season. *Int. J. Environ. Res. Public Health* **12**, 13649–13661 (2015).
20. Stegen, J. C. et al. Groundwater-surface water mixing shifts ecological assembly processes and stimulates organic carbon turnover. *Nat. Commun.* **7**, 11237 (2016).
21. Lima-Mendez, G. et al. Determinants of community structure in the global plankton interactome. *Science* **348**, 1262073 (2015).
22. Chaffron, S. et al. Environmental vulnerability of the global ocean epipelagic plankton community interactome. *Sci. Adv.* **7**, eabg1921 (2021).
23. Revetta, R. P., Pemberton, A., Lamendella, R., Iker, B. & Santo Domingo, J. W. Identification of bacterial populations in drinking water using 16S rRNA-based sequence analyses. *Water Res.* **44**, 1353–1360 (2010).
24. Chen, L., Li, X., Medema, G., van der Meer, W. & Liu, G. Transition effects in an unchlorinated drinking water system following the introduction of partial reverse osmosis. *Nat. Water* **1**, 961–970 (2023).
25. Zhang, L. et al. Daily sampling reveals household-specific water microbiome signatures and shared antimicrobial resistomes in premise plumbing. *Nat. Water* **2**, 1178–1194 (2024).
26. Hou, C., Chen, L., Dong, Y., Yang, Y. & Zhang, X. Unraveling dissolved organic matter in drinking water through integrated ozonation/ceramic membrane and biological activated carbon process using FT-ICR MS. *Water Res.* **222**, 118881 (2022).
27. Xu, W. et al. Using ESI FT-ICR MS to characterize dissolved organic matter in salt lakes with different salinity. *Environ. Sci. Technol.* **54**, 12929–12937 (2020).
28. Zark, M. & Dittmar, T. Universal molecular structures in natural dissolved organic matter. *Nat. Commun.* **9**, 3178 (2018).
29. Hu, A. et al. Ecological networks of dissolved organic matter and microorganisms under global change. *Nat. Commun.* **13**, 3600 (2022).
30. Freeman, E. C. et al. Universal microbial reworking of dissolved organic matter along environmental gradients. *Nat. Commun.* **15**, 187 (2024).
31. Hu, J. et al. Photo-produced aromatic compounds stimulate microbial degradation of dissolved organic carbon in thermokarst lakes. *Nat. Commun.* **14**, 3681 (2023).
32. Al-Jasser, A. O. Chlorine decay in drinking-water transmission and distribution systems: pipe service age effect. *Water Res.* **41**, 387–396 (2007).
33. Siebel, E., Wang, Y., Egli, T. & Hammes, F. Correlations between total cell concentration, total adenosine tri-phosphate concentration and heterotrophic plate counts during microbial monitoring of drinking water. *Drinking Water Eng. Sci.* **1**, 1–6 (2008).
34. Li, B., Chen, X., Yang, J. Y., Gao, S. & Bai, F. Intracellular ATP concentration is a key regulator of bacterial cell fate. *J. Bacteriol.* **206**, e0020824 (2024).

35. Liu, G. et al. Assessing the origin of bacteria in tap water and distribution system in an unchlorinated drinking water system by SourceTracker using microbial community fingerprints. *Water Res.* **138**, 86–96 (2018).
36. Chen, L., Li, X., van der Meer, W., Medema, G. & Liu, G. Capturing and tracing the spatiotemporal variations of planktonic and particle-associated bacteria in an unchlorinated drinking water distribution system. *Water Res.* **219**, 118589 (2022).
37. Liu, G. et al. Pyrosequencing reveals bacterial communities in unchlorinated drinking water distribution system: an integral study of bulk water, suspended solids, loose deposits, and pipe wall biofilm. *Environ. Sci. Technol.* **48**, 5467–5476 (2014).
38. Yao, M. et al. Building water quality deterioration during water supply restoration after interruption: Influences of premise plumbing configuration. *Water Res.* **241**, 120149 (2023).
39. Wang, H. et al. Microbial community response to chlorine conversion in a chloraminated drinking water distribution system. *Environ. Sci. Technol.* **48**, 10624–10633 (2014).
40. Hwang, C., Ling, F., Andersen, G. L., LeChevallier, M. W. & Liu, W. T. Microbial community dynamics of an urban drinking water distribution system subjected to phases of chloramination and chlorination treatments. *Appl. Environ. Microbiol.* **78**, 7856–7865 (2012).
41. Park, H. D. & Noguera, D. R. Evaluating the effect of dissolved oxygen on ammonia-oxidizing bacterial communities in activated sludge. *Water Res.* **38**, 3275–3286 (2004).
42. Lesaulnier, C. C. et al. Bottled aqua incognita: microbiota assembly and dissolved organic matter diversity in natural mineral waters. *Microbiome* **5**, 126 (2017).
43. Logue, J. B. et al. Experimental insights into the importance of aquatic bacterial community composition to the degradation of dissolved organic matter. *ISME J.* **10**, 533–545 (2016).
44. Rahmatika, I., Simazaki, D., Kurisu, F., Furumai, H. & Kasuga, I. Occurrence and diversity of nontuberculous mycobacteria affected by water stagnation in building plumbing. *Water Supply* **23**, 5017–5028 (2023).
45. Lin, H., Szeinbaum, N. H., DiChristina, T. J. & Taillefert, M. Microbial Mn(IV) reduction requires an initial one-electron reductive solubilization step. *Geochim. Cosmochim. Acta* **99**, 179–192 (2012).
46. Li, G. et al. Field studies of manganese deposition and release in drinking water distribution systems: Insight into deposit control. *Water Res.* **163**, 114897 (2019).
47. Omran, A. M., Abdel-Jaber, G. T. & Ali, M. M. Effect of Cu and Mn on the mechanical properties and microstructure of ductile cast iron. *J. Eng. Res. Appl.* **4**, 90–96 (2014).
48. Tian, T. et al. Distinct and diverse anaerobic respiration of methanogenic community in response to MnO_2 nanoparticles in anaerobic digester sludge. *Water Res.* **123**, 206–215 (2017).
49. Yao, W. & Millero, F. J. The rate of sulfide oxidation by δMnO_2 in seawater. *Geochim. Cosmochim. Acta* **57**, 3359–3365 (1993).
50. Carbonell-Barrachina, A. A., Jugsujinda, A., Burlo, F., Delaune, R. D. & Patrick, W. H. Arsenic chemistry in municipal sewage sludge as affected by redox potential and pH. *Water Res.* **34**, 216–224 (2000).
51. Masscheleyn, P. H., Delaune, R. D. & Patrick, W. H. Effect of redox potential and pH on arsenic speciation and solubility in a contaminated soil. *Environ. Sci. Technol.* **25**, 1414–1419 (2002).
52. Cheng, X. et al. Polarity-based fractionation and identification of high-toxicity disinfection by-product precursors in drinking water. *Water Res.* **286**, 124204 (2025).
53. LaRowe, D. E. & Van Cappellen, P. Degradation of natural organic matter: a thermodynamic analysis. *Geochim. Cosmochim. Acta* **75**, 2030–2042 (2011).
54. Chen, X. et al. Oxygen availability driven trends in DOM molecular composition and reactivity in a seasonally stratified fjord. *Water Res.* **220**, 118690 (2022).
55. Tao, Y., Du, Y., Deng, Y., Ma, T. & Wang, Y. Degradation of phosphorus-containing natural organic matter facilitates enrichment of geogenic phosphorus in Quaternary aquifer systems: a molecular perspective. *J. Hydrol.* **620**, 129513 (2023).
56. Jessen, G. L. et al. Hypoxia causes preservation of labile organic matter and changes seafloor microbial community composition (Black Sea). *Sci. Adv.* **3**, e1601897 (2017).
57. LaBrie, R. et al. Deep ocean microbial communities produce more stable dissolved organic matter through the succession of rare prokaryotes. *Sci. Adv.* **8**, eabn0035 (2022).
58. Li, H. Y. et al. The chemodiversity of paddy soil dissolved organic matter correlates with microbial community at continental scales. *Microbiome* **6**, 187 (2018).
59. Ren, X. & Chen, H. Effect of residual chlorine on the interaction between bacterial growth and assimilable organic carbon and biodegradable organic carbon in reclaimed water. *Sci. Total Environ.* **752**, 141223 (2021).
60. Xu, H. et al. Molecular characteristics of dissolved organic nitrogen and its interaction with microbial communities in a prechlorinated raw water distribution system. *Environ. Sci. Technol.* **54**, 1484–1492 (2020).
61. Tanentzap, A. J. et al. Chemical and microbial diversity covary in fresh water to influence ecosystem functioning. *Proc. Natl Acad. Sci. USA* **116**, 24689–24695 (2019).
62. Danczak, R. E. et al. Using metacommunity ecology to understand environmental metabolomes. *Nat. Commun.* **11**, 6369 (2020).
63. Zhou, J. & Ning, D. Stochastic community assembly: does it matter in microbial ecology?. *Microbiol. Mol. Biol. Rev.* **81**, e00002–e00017 (2017).
64. Freire-Zapata, V. et al. Microbiome–metabolite linkages drive greenhouse gas dynamics over a permafrost thaw gradient. *Nat. Microbiol.* **9**, 2892–2908 (2024).
65. Ma, K. et al. Disentangling drivers of mudflat intertidal DOM chemodiversity using ecological models. *Nat. Commun.* **15**, 6620 (2024).
66. Ning, D. et al. Environmental stress mediates groundwater microbial community assembly. *Nat. Microbiol.* **9**, 490–501 (2024).
67. Deng, Y. et al. Molecular ecological network analyses. *BMC Bioinf.* **13**, 113 (2012).
68. Luo, F., Zhong, J., Yang, Y. & Zhou, J. Application of random matrix theory to microarray data for discovering functional gene modules. *Phys. Rev. E* **73**, 031924 (2006).
69. Yang, J. et al. Potential utilization of terrestrially derived dissolved organic matter by aquatic microbial communities in saline lakes. *ISME J.* **14**, 2313–2324 (2020).
70. Yu, S. et al. Changes of soil dissolved organic matter and its relationship with microbial community along the Hailuogou glacier forefield chronosequence. *Environ. Sci. Technol.* **57**, 4027–4038 (2023).
71. Park, J. W. et al. Occurrences and changes in bacterial growth-promoting nutrients in drinking water from source to tap: a review. *Environ. Sci. Water Res. Technol.* **7**, 2206–2222 (2021).
72. Nescerecka, A., Juhna, T. & Hammes, F. Identifying the underlying causes of biological instability in a full-scale drinking water supply system. *Water Res.* **135**, 11–21 (2018).
73. Chen, X. et al. Niche differentiation of microbial community shapes vertical distribution of recalcitrant dissolved organic matter in deep-sea sediments. *Environ. Int.* **178**, 108080 (2023).
74. Zhou, L. et al. Resource aromaticity affects bacterial community successions in response to different sources of dissolved organic matter. *Water Res.* **190**, 116776 (2021).

75. Rodríguez-Ramos, T., Nieto-Cid, M., Auladell, A., Guerrero-Feijóo, E. & Varela, M. M. Vertical niche partitioning of archaea and bacteria linked to shifts in dissolved organic matter quality and hydrography in North Atlantic waters. *Front. Mar. Sci.* **8**, 673171 (2021).
76. Prest, E. I., Hammes, F., van Loosdrecht, M. C. & Vrouwenvelder, J. S. Biological stability of drinking water: controlling factors, methods, and challenges. *Front. Microbiol.* **7**, 45 (2016).
77. Chan, S. et al. Bacterial release from pipe biofilm in a full-scale drinking water distribution system. *NPJ Biofilms Microbiomes* **5**, 9 (2019).
78. Shah Walter, S. R. et al. Microbial decomposition of marine dissolved organic matter in cool oceanic crust. *Nat. Geosci.* **11**, 334–339 (2018).
79. Catalan, N. et al. Treeline displacement may affect lake dissolved organic matter processing at high latitudes and altitudes. *Nat. Commun.* **15**, 2640 (2024).
80. Hammes, F. A. & Egli, T. New method for assimilable organic carbon determination using flow-cytometric enumeration and a natural microbial consortium as inoculum. *Environ. Sci. Technol.* **39**, 3289–3294 (2005).
81. Hammes, F. et al. Flow-cytometric total bacterial cell counts as a descriptive microbiological parameter for drinking water treatment processes. *Water Res.* **42**, 269–277 (2008).
82. Nescerecka, A., Hammes, F. & Juhna, T. A pipeline for developing and testing staining protocols for flow cytometry, demonstrated with SYBR Green I and propidium iodide viability staining. *J. Microbiol. Methods* **131**, 172–180 (2016).
83. Fan, M. et al. Disruptive effects of sewage intrusion into drinking water: microbial succession and organic transformation at molecular level. *Water Res.* **266**, 122281 (2024).
84. Ezzat, L. et al. Diversity and biogeography of the bacterial microbiome in glacier-fed streams. *Nature* **637**, 622–630 (2025).
85. Martin, M. Cutadapt removes adapter sequences from high-throughput sequencing reads. *EMBnet J.* **17**, 10–12 (2011).
86. Callahan, B. J. et al. DADA2: high-resolution sample inference from Illumina amplicon data. *Nat. Methods* **13**, 581–583 (2016).
87. Bolyen, E. et al. Reproducible, interactive, scalable and extensible microbiome data science using QIIME 2. *Nat. Biotechnol.* **37**, 852–857 (2019).
88. Underwood, G. J. C. et al. Organic matter from Arctic sea-ice loss alters bacterial community structure and function. *Nat. Clim. Change* **9**, 170–176 (2019).
89. Ohno, T. Fluorescence inner-filtering correction for determining the humification index of dissolved organic matter. *Environ. Sci. Technol.* **36**, 742–746 (2002).
90. Pucher, M. et al. staRdom: versatile software for analyzing spectroscopic data of dissolved organic matter in R. *Water* **11**, 2366 (2019).
91. Gonsior, M. et al. Changes in dissolved organic matter during the treatment processes of a drinking water plant in Sweden and formation of previously unknown disinfection byproducts. *Environ. Sci. Technol.* **48**, 12714–12722 (2014).
92. Boutegrabet, L. et al. Attachment of chloride anion to sugars: mechanistic investigation and discovery of a new dopant for efficient sugar ionization/detection in mass spectrometers. *Chemistry* **18**, 13059–13067 (2012).
93. Dixon, P. VEGAN, a package of R functions for community ecology. *J. Veget. Sci.* **14**, 927–930 (2003).
94. Ning, D., Deng, Y., Tiedje, J. M. & Zhou, J. A general framework for quantitatively assessing ecological stochasticity. *Proc. Natl Acad. Sci. USA* **116**, 16892–16898 (2019).
95. Stegen, J. C. et al. Quantifying community assembly processes and identifying features that impose them. *ISME J.* **7**, 2069–2079 (2013).
96. Stegen, J. C., Lin, X., Fredrickson, J. K. & Konopka, A. E. Estimating and mapping ecological processes influencing microbial community assembly. *Front. Microbiol.* **6**, 370 (2015).
97. Benjamini, Y. & Hochberg, Y. Controlling the false discovery rate: a practical and powerful approach to multiple testing. *J. R. Stat. Soc. Ser. B* **57**, 289–300 (1995).
98. Guimera, R. & Nunes Amaral, L. A. Functional cartography of complex metabolic networks. *Nature* **433**, 895–900 (2005).
99. Fan, M. et al. Stagnant water in fire hydrant branches: overlooked chemical–microbial coupled deterioration in drinking water distribution systems. *Zenodo* https://doi.org/10.5281/zenodo.17422657 (2025).
100. Batista-Andrade, J. A. et al. Spatiotemporal analysis of fluorescent dissolved organic matter to identify the impacts of failing sewer infrastructure in urban streams. *Water Res.* **229**, 119521 (2023).
101. Osburn, C. L., Handsel, L. T., Mikan, M. P., Paerl, H. W. & Montgomery, M. T. Fluorescence tracking of dissolved and particulate organic matter quality in a river-dominated estuary. *Environ. Sci. Technol.* **46**, 8628–8636 (2012).
102. Lei, J., Yang, L. & Zhu, Z. Testing the effects of coastal culture on particulate organic matter using absorption and fluorescence spectroscopy. *J. Clean. Prod.* **325**, 129203 (2021).
103. D'Andrilli, J., Junker, J. R., Smith, H. J., Scholl, E. A. & Foreman, C. M. DOM composition alters ecosystem function during microbial processing of isolated sources. *Biogeochemistry* **142**, 281–298 (2019).
104. Osburn, C. L., Handsel, L. T., Peierls, B. L. & Paerl, H. W. Predicting sources of dissolved organic nitrogen to an estuary from an agro-urban coastal watershed. *Environ. Sci. Technol.* **50**, 8473–8484 (2016).
105. Amaral, V., Romera-Castillo, C. & Forja, J. Submarine mud volcanoes as a source of chromophoric dissolved organic matter to the deep waters of the Gulf of Cadiz. *Sci. Rep.* **11**, 3200 (2021).
106. Hambly, A. C. et al. Characterising organic matter in recirculating aquaculture systems with fluorescence EEM spectroscopy. *Water Res.* **83**, 112–120 (2015).
107. Hambly, A. C. et al. Fluorescence monitoring at a recycled water treatment plant and associated dual distribution system—implications for cross-connection detection. *Water Res.* **44**, 5323–5333 (2010).
108. Lee, D. et al. Characteristics of intracellular algogenic organic matter and its reactivity with hydroxyl radicals. *Water Res.* **144**, 13–25 (2018).

Acknowledgements

The present work has been financially supported by the National Natural Science Foundation of China (grant nos. 52388101, 52525003 and 52370105 to G.L.; 52170105 to Q.X.).

Author contributions

M.F. led the sampling strategy development, data acquisition, data analysis and manuscript writing. Q.X. contributed equally to strategy development and data acquisition, assisted in data analysis and provided overall guidance. X.W. and Z.F. assisted with data acquisition. M.C.M.V.L. and M.P. provided guidance on data analysis and writing. Y.T., J.B.R. and W.V.D.M. contributed editorial and writing guidance. G.L. supervised the entire project from scientific design to data analysis and also contributed to manuscript writing.

Competing interests

The authors declare no competing interests.

Additional information

Supplementary information The online version contains supplementary material available at https://doi.org/10.1038/s44221-025-00542-4.

Correspondence and requests for materials should be addressed to Gang Liu.

Peer review information *Nature Water* thanks Hans-Jørgen Albrechtsen, Weiyi Pan and the other, anonymous, reviewer(s) for their contribution to the peer review of this work.

nature portfolio

Corresponding author(s): Gang Liu

Last updated by author(s): Oct 24, 2025

Reporting Summary

Nature Portfolio wishes to improve the reproducibility of the work that we publish. This form provides structure for consistency and transparency in reporting. For further information on Nature Portfolio policies, see our Editorial Policies and the Editorial Policy Checklist.

Statistics

For all statistical analyses, confirm that the following items are present in the figure legend, table legend, main text, or Methods section.

n/a	Confirmed
☐	☒ The exact sample size (*n*) for each experimental group/condition, given as a discrete number and unit of measurement
☐	☒ A statement on whether measurements were taken from distinct samples or whether the same sample was measured repeatedly
☐	☒ The statistical test(s) used AND whether they are one- or two-sided *Only common tests should be described solely by name; describe more complex techniques in the Methods section.*
☒	☐ A description of all covariates tested
☐	☒ A description of any assumptions or corrections, such as tests of normality and adjustment for multiple comparisons
☐	☒ A full description of the statistical parameters including central tendency (e.g. means) or other basic estimates (e.g. regression coefficient) AND variation (e.g. standard deviation) or associated estimates of uncertainty (e.g. confidence intervals)
☐	☒ For null hypothesis testing, the test statistic (e.g. *F*, *t*, *r*) with confidence intervals, effect sizes, degrees of freedom and *P* value noted *Give P values as exact values whenever suitable.*
☒	☐ For Bayesian analysis, information on the choice of priors and Markov chain Monte Carlo settings
☐	☒ For hierarchical and complex designs, identification of the appropriate level for tests and full reporting of outcomes
☐	☒ Estimates of effect sizes (e.g. Cohen's *d*, Pearson's *r*), indicating how they were calculated

Our web collection on statistics for biologists contains articles on many of the points above.

Software and code

Policy information about availability of computer code

Data collection	No software was used.
Data analysis	EEM data by the StaRDOM(1.1.28) package;Ecological Assembly Process by NST(3.1.10) package;Co-occurrence network by Gephi(0.10.1);All the statistical analyses were performed in R (version 4.3.1, R Core Team, 2023).

For manuscripts utilizing custom algorithms or software that are central to the research but not yet described in published literature, software must be made available to editors and reviewers. We strongly encourage code deposition in a community repository (e.g. GitHub). See the Nature Portfolio guidelines for submitting code & software for further information.

Data

Policy information about availability of data

All manuscripts must include a data availability statement. This statement should provide the following information, where applicable:

- Accession codes, unique identifiers, or web links for publicly available datasets
- A description of any restrictions on data availability
- For clinical datasets or third party data, please ensure that the statement adheres to our policy

The sequencing data have been deposited in the NCBI database and publicly available, with reference code PRJNA1267700.

Research involving human participants, their data, or biological material

Policy information about studies with human participants or human data. See also policy information about sex, gender (identity/presentation), and sexual orientation and race, ethnicity and racism.

Reporting on sex and gender	Not applicable.
Reporting on race, ethnicity, or other socially relevant groupings	Not applicable.
Population characteristics	Not applicable.
Recruitment	Not applicable.
Ethics oversight	Not applicable.

Note that full information on the approval of the study protocol must also be provided in the manuscript.

Field-specific reporting

Please select the one below that is the best fit for your research. If you are not sure, read the appropriate sections before making your selection.

☐ Life sciences ☐ Behavioural & social sciences ☒ Ecological, evolutionary & environmental sciences

For a reference copy of the document with all sections, see nature.com/documents/nr-reporting-summary-flat.pdf

Ecological, evolutionary & environmental sciences study design

All studies must disclose on these points even when the disclosure is negative.

Study description	This study was conducted in a city in northern China. Water samples were collected from stagnant water in fire hydrants and their branch pipes at 15 locations, as well as from flowing water in the corresponding main pipes. The primary objective was to reveal, through comparison, that hydrants, as non-consumer terminals, may represent overlooked yet widespread risk nodes in drinking water distribution systems. Each type of water at each location was sampled in triplicate (n = 15 × 2 × 3 = 90).
Research sample	Research samples include stagnant water in fire hydrants and the corresponding flowing water from the main pipes.
Sampling strategy	During sampling, the fire hydrant was first fully opened to allow high-pressure water to flush out potential contaminants from around and inside the hydrant outlet. After a few seconds, the valve was partially closed to allow stagnant water to flow out steadily. Once the flow stabilized, the stagnant water sample was collected. After sampling, the hydrant was fully reopened to flush out any remaining stagnant water. When the water ran clear and a chlorine odor was detectable, the hydrant was allowed to flow steadily for an additional 10 minutes before the flowing water sample was collected.
Data collection	The basic physicochemical and microbiological water quality parameters were measured by the authors (Mengqing Fan, Xiaoxuan Wang, Zhiwei Fang) in a laboratory. Microbial DNA extraction and pretreatment of samples for FT-ICR MS analysis were performed by the first author (Mengqing Fan) in a professional laboratory. DNA sequencing was conducted by Guangdong Magigene Biotechnology Co., Ltd. FT-ICR MS data acquisition was carried out by Mengqing Fan with assistance from professional laboratory technicians. All data processing was performed by the authors on an in-house workstation.
Timing and spatial scale	For spatial scale, we selected representative sites covering a broad geographic range—from the city center to suburban areas and from northern to southern regions.
Data exclusions	No data were excluded from the analyses.
Reproducibility	All the samples were taken carefully in triplicates. All attempts to repeat the experiment were successful.
Randomization	No experimental allocation or randomization was applied, as the study groups were predetermined at the time of sample collection.
Blinding	No blinding was applied, as samples were collected from clearly identifiable locations and all measurements were objective and instrument-based.

Did the study involve field work? ☒ Yes ☐ No

Field work, collection and transport

Field conditions	This study was conducted in a city in northern China, where the municipal drinking water supply is primarily sourced from both surface water and groundwater. The supplied water undergoes a comprehensive treatment process, including pre-ozonation, coagulation, sedimentation, sand filtration, activated carbon filtration, and disinfection. The city has approximately 81,000 fire hydrants, which are installed underground, distributed throughout the drinking water distribution system.
Location	Samples were collected within a longitude range of 116.15 to 116.61 and a latitude range of 39.99 to 40.13.
Access & import/export	Samples were collected with the assistance of the local water utility, in full compliance with all applicable regulations, without affecting the normal water supply.
Disturbance	No disturbance was caused by the study.

Reporting for specific materials, systems and methods

We require information from authors about some types of materials, experimental systems and methods used in many studies. Here, indicate whether each material, system or method listed is relevant to your study. If you are not sure if a list item applies to your research, read the appropriate section before selecting a response.

Materials & experimental systems

n/a	Involved in the study
☒	☐ Antibodies
☒	☐ Eukaryotic cell lines
☒	☐ Palaeontology and archaeology
☒	☐ Animals and other organisms
☒	☐ Clinical data
☒	☐ Dual use research of concern
☒	☐ Plants

Methods

n/a	Involved in the study
☒	☐ ChIP-seq
☐	☒ Flow cytometry
☒	☐ MRI-based neuroimaging

Plants

Seed stocks	n/a
Novel plant genotypes	n/a
Authentication	n/a

Flow Cytometry

Plots

Confirm that:

☐ The axis labels state the marker and fluorochrome used (e.g. CD4-FITC).

☐ The axis scales are clearly visible. Include numbers along axes only for bottom left plot of group (a 'group' is an analysis of identical markers).

☐ All plots are contour plots with outliers or pseudocolor plots.

☒ A numerical value for number of cells or percentage (with statistics) is provided.

Methodology

Sample preparation	Samples (1 mL) were stained with 10 µL mL−1 SYBR® Green I (1:100 dilution in DMSO; Molecular Probes) and incubated in the dark for 10 min at 35 °C before measurement. Flow cytometric measurements were performed, using an Agilent NovoCyte 1040® (NovoCyte, USA).

Instrument	Agilent NovoCyte 1040® (NovoCyte, USA)
Software	NovoExpress
Cell population abundance	Total cells were enumerated using SYBR Green I, with abundances ranging from 10^3 to 10^7 cells/mL.
Gating strategy	We used several samples to optimize instrument settings during data acquisition. These settings were then saved and applied consistently to all samples.

☐ Tick this box to confirm that a figure exemplifying the gating strategy is provided in the Supplementary Information.